APPLIED PHYSICS

Inferring non-equilibrium interactions from tracer response near confined active Janus particles

Jaideep Katuri[1]*, William E. Uspal[2,3]*, Mihail N. Popescu[3]*, Samuel Sánchez[1,4]*

Chemically active Janus particles sustain non-equilibrium spatial variations in the chemical composition of the suspending solution; these induce hydrodynamic flow and (self-)motility of the particles. Direct mapping of these fields has so far proven to be too challenging. Therefore, indirect methods are needed, e.g., deconvolving the response of "tracer" particles to the activity-induced fields. Here, we study experimentally the response of silica particles, sedimented at a wall, to active Pt/silica Janus particles. The latter are either immobilized at the wall, with the symmetry axis perpendicular or parallel to the wall, or motile. The experiments reveal complex effective interactions that are dependent on the configuration and on the state of motion of the active particle. Within the framework of a coarse-grained model, the behavior of tracers near an immobilized Janus particle can be captured qualitatively once activity-induced osmotic flows on the wall are considered.

INTRODUCTION

Colloidal particles that can autonomously harvest energy from their environment to power their motion through a viscous fluid (*1*, *2*) are an important example of synthetic active matter systems (*3*). A rich variety of non-equilibrium phenomena have been observed to emerge in these systems, either spontaneously or in response to external stimuli. These are governed by the interplay between self-propulsion, thermal fluctuations, and pairwise interactions (equilibrium and non-equilibrium) among active particles and with nearby interfaces. The non-equilibrium, effective interactions occur through the local coupling of the fields (e.g., hydrodynamic and chemical) sourced by the chemical activity of the particle, and they govern the dynamics observed in systems of active particles. Ensembles of active particles have been shown to form, depending on the details of these effective interactions, directional flocks (*4*) and motile vortices (*5*), as well as self-assembled dynamic crystalline structures (*6*–*9*) or self-spinning rotors (*10*). It is even possible to switch between different states of collective motion by dynamically modifying these interactions (*11*). Furthermore, studies of mixtures of dopant active particles in a bath of passive particles (*12*) revealed the potential of these systems for self-assembly, i.e., clustering around the active particle (*13*), and gel formation (*14*).

When a chemically active particle moves in the vicinity of a wall, the confinement distorts the chemical and hydrodynamic fields, which qualitatively affects the dynamics of the particle (*15*–*18*). Active particles can change their orientation in response to a nearby surface and have been shown to accumulate along walls (*19*). In the presence of topographical patterns, an active alignment along these structures emerges even if the feature height is substantially smaller than the radius of the particle (*20*). This reorientation mechanism can be exploited to guide self-propelled particles along predefined paths (*19*, *20*), assemble them into microgear structures (*21*), and generate a directional flow of particles even at dilute concentrations (*22*). Furthermore, a strong directional response results when an external flow couples to a surface-bound, sliding active particle, leading to particle rheotaxis (*23*) and cross-stream migration (*24*).

While the hydrodynamic and chemical fields play a dominant role in determining both the collective dynamics of active systems and their response to external perturbations, very few studies have been performed to trace these fields and to study the resulting interactions in detail (*25*–*27*). The role of confinement on the effective interactions between particles has been, in general, overlooked, although most synthetic active systems are composed of density-mismatched particles that operate close to the bottom surface (*6*, *20*) or are antigravitactic and swim to accumulate at the top surface (*26*, *28*, *29*). An understanding of the role that confining surfaces play in determining particle interactions will also enable rational design of surface properties to achieve spatially confined steady-state dynamics in active systems (*30*, *31*).

In this study, we use the response of spherical, inert silica particles (tracers) to investigate the nature of the hydrodynamic and chemical fields associated with the chemical activity of a spherical Pt-silica Janus particle. We use active particles that are immobilized with the symmetry axis being either perpendicular or parallel to the wall, as well as active particles that are sliding along the wall (thus in an axis-parallel configuration). This allows us to address the effect of the confining wall on the effective interactions experienced by the tracers, and the dependence of the effective interactions on the configuration of the active particle. In this manner, qualitatively distinct, configuration-dependent, responses of the tracers are evidenced. For example, for an immobile active particle in an axis-perpendicular configuration, tracers are attracted to the active particle; but for an immobile active particle in an axis-parallel configuration, a notably anisotropic response emerges: The tracer particles accumulate at the inert side of the Janus particle, while a tracer-free exclusion zone surrounds the Pt side. The tracer motion in the case of immobilized Janus particles is amenable to theoretical analysis at the single-particle level (dilute limit). We show that the experimental observations can be qualitatively captured and rationalized by a simple model of a chemically active particle. This requires accounting for the distortion by the wall of the hydrodynamic and chemical fields around the particle, as well as for an osmotic flow at the wall in response to the

[1]Institute for Bioengineering of Catalonia (IBEC), The Barcelona Institute of Science and Technology (BIST), Baldiri Reixac 10-12, 08028 Barcelona Spain. [2]Department of Mechanical Engineering, University of Hawaii at Manoa, 2540 Dole Street, Holmes Hall 302, Honolulu, HI 96822, USA. [3]Max-Planck-Institut für Intelligente Systeme, Heisenbergstr. 3, D-70569 Stuttgart, Germany. [4]Institució Catalana de Recerca i Estudis Avancats (ICREA), Pg. Lluís Companys 23, 08010 Bacelona, Spain.
*Corresponding author. Email: ssanchez@ibecbarcelona.eu (S.S.); jkaturi@anl.gov (J.K.); popescu@is.mpg.de (M.N.P.); uspal@hawaii.edu (W.E.U.)

chemical activity of the particle. The latter is further supported by additional experiments with the same particles and tracers but walls made of different materials, which demonstrate that the response of the tracers depends on the material of the wall.

RESULTS

Experimental setup

The chemically active Janus particles used in our experiments are spherical silica beads of radius $R = 2.5$ μm half-covered with a thin layer of Pt (see Methods). We define the orientation of the Janus particle via the unit vector **d**, which lies along the symmetry axis and is oriented from the chemically active hemisphere to the inactive one. As tracers, we use chemically inactive silica particles of radii $R_{tr} = 1$ μm or $R_{tr} = 0.5$ μm.

For an experiment, a drop of an aqueous suspension of tracers (of one size) is deposited onto a glass slide, on which Janus particles are adhered with their symmetry axis in various configurations (for details, see Methods), including the desired axis-perpendicular and axis-parallel ones. By varying the volume fraction of the silica tracers in the suspension, dilute or dense (closed packed) in-plane monolayers of tracers, as needed for a particular setup (see below), can be formed upon sedimentation.

As long as no H_2O_2 is added to the solution (i.e., there is no chemical activity), the tracers display regular Brownian motion, with negligible out-of-plane fluctuations and no interaction (other than hard-core steric repulsion) is observed between the particles (see Fig. 1A, left). Upon addition of H_2O_2, i.e., once the chemical activity is turned on, it is observed that some of the stuck Janus particles detach and start moving along the glass slide, with the Pt cap at the back. However, many of the Janus particles remain stuck in configurations with the symmetry axis parallel or perpendicular to the glass slide. Consequently, each such experimental realization allows, in general, simultaneous observations of three situations involving a chemically active particle: immobile Janus particle (stuck to the wall) in an axis parallel or axis perpendicular to the wall configuration, and mobile Janus particle in a sliding state.

Experiment: Active Janus particle stuck to the wall

We first discuss the experimental observations in the case of immobile active Janus particles that are stuck to the wall. The two configurations of interest, i.e., cap-perpendicular and cap-parallel, are presented and analyzed in the following.

Axis-perpendicular configuration

We start the discussion with the observations in the case of the tracer particles of radius $R_{tr} = 1$ μm. For a Janus particle stuck with the symmetry axis perpendicular to the wall, it is observed that, upon addition of H_2O_2, silica tracers located in the vicinity of the particle are drawn toward it (see Fig. 1, B and C). (Note that the optical microscopy observations cannot discriminate whether this is a cap-up or a cap-down configuration.) This implies that the chemical activity of the Janus particle is experienced by the tracers as an effective attraction (see Fig. 1C). The magnitude of this interaction is substantial (in the sense that it dominates thermal fluctuations) over a spatial range of few radii of the Janus particle; the interaction is sufficiently strong to lead to quasi-crystalline ring structures around the active Janus particle (see Fig. 1, B and C, and movie S1). As shown in Fig. 1B, during the formation of the ring structure, the motion of a drawn-in tracer is basically along the radial direction until it reaches the active particle, after which it translates within the (yet to be completely filled) ring along the circumference. The observation of strongly biased motion is consistent with an estimate $Pe_t \gg 1$ for the tracer Péclet number $Pe_t := |\mathbf{v}_t| R_{tr}/D_{tr}$, where D_{tr} is the diffusion constant of the tracer and $\mathbf{v}_t$ is the tracer velocity. From analysis of the data in Fig. 1, we estimate that $|\mathbf{v}_t| \sim 5$ μm/s is a typical magnitude of the tracer velocity. Accordingly, for an $R_{tr} = 1$ μm tracer immersed in water, we estimate $Pe_t \approx 20$. (Note that this estimate does not account for hindrance of tracer diffusion by the wall, which would lower D_{tr}, i.e., increase Pe_t by a prefactor ~2 to 3 that depends on the height of the tracer above the wall.)

Once the first ring is completely filled, the compact ring structure turns stable (no tracer leaves the ring); however, tracers are still drawn in and additional ring structures build, ring after ring, around the active particle (see Fig. 1C). The number of rings formed depends on the concentration of H_2O_2, i.e., on the activity; at low concentrations of H_2O_2 ($\lesssim$2%), a single ring forms, while at high concentrations of H_2O_2 ($\simeq$6%, i.e., the value above which the velocity of a motile Janus particle becomes roughly independent of the H_2O_2 concentration), three to four rings form around the Janus particle (Fig. 1D). The tracers closer to the Janus particle are more tightly confined compared to those further away, as can be inferred from the corresponding trajectories and mean square displacements (see Fig. 1, E and F). Last, one notes that there are occasional exchanges of tracers between the outermost ring and the "bulk" solution, but there is no exchange of particles involving the inner concentric rings once they are completely filled. The structure remains stable for hours (more precisely, for as long as sufficient H_2O_2 is in the solution) but melts away once the system runs out of H_2O_2. This further argues for the dynamic, activity-induced nature of the ring structure.

Concerning the experiments with the smaller tracer particles (radius $R_{tr} = 0.5$ μm), they reveal a similar behavior where four to six rings form around the Janus particle at $H_2O_2 \simeq 6\%$ (see Fig. 1, G and H, and movie 2). Similar to the case of larger tracer particles, these structures remain stable for as long as there is sufficient H_2O_2 in the solution.

Axis-parallel configuration

We turn next to the behavior exhibited by passive silica tracers in the vicinity of an active Janus particle stuck at the wall in an axis-parallel configuration (Fig. 2). The areal density of tracers was suitably adjusted to reach a compromise between keeping the system in the dilute monolayer limit while still having sufficiently many tracers around a stuck active particle to allow a mapping of the attraction and repulsion regions.

Immediately upon addition of H_2O_2, tracers that are initially located in a cone-like region opening from the inert side of the Janus particle are rapidly drawn toward the inert cap. This leads to the formation of circular segments of rings of passive particles on the silica side of the active particle (see Fig. 2, A and C), bearing resemblance with the compact-to-loose multiring structures observed for the case of the active particle stuck in an axis-perpendicular configuration. A plot of the steady-state distribution of tracer particles around the silica half reveals that the closest ring of particles is more tightly bound as compared to the outer rings (Fig. 2, B and D). These circular segments end near the equator region (the circle separating the active and passive caps) of the Janus particle, somewhat into the chemically active region.

At the Pt side of the particle, an opposite effect (i.e., a repulsive interaction) is observed, and an exclusion zone, completely depleted

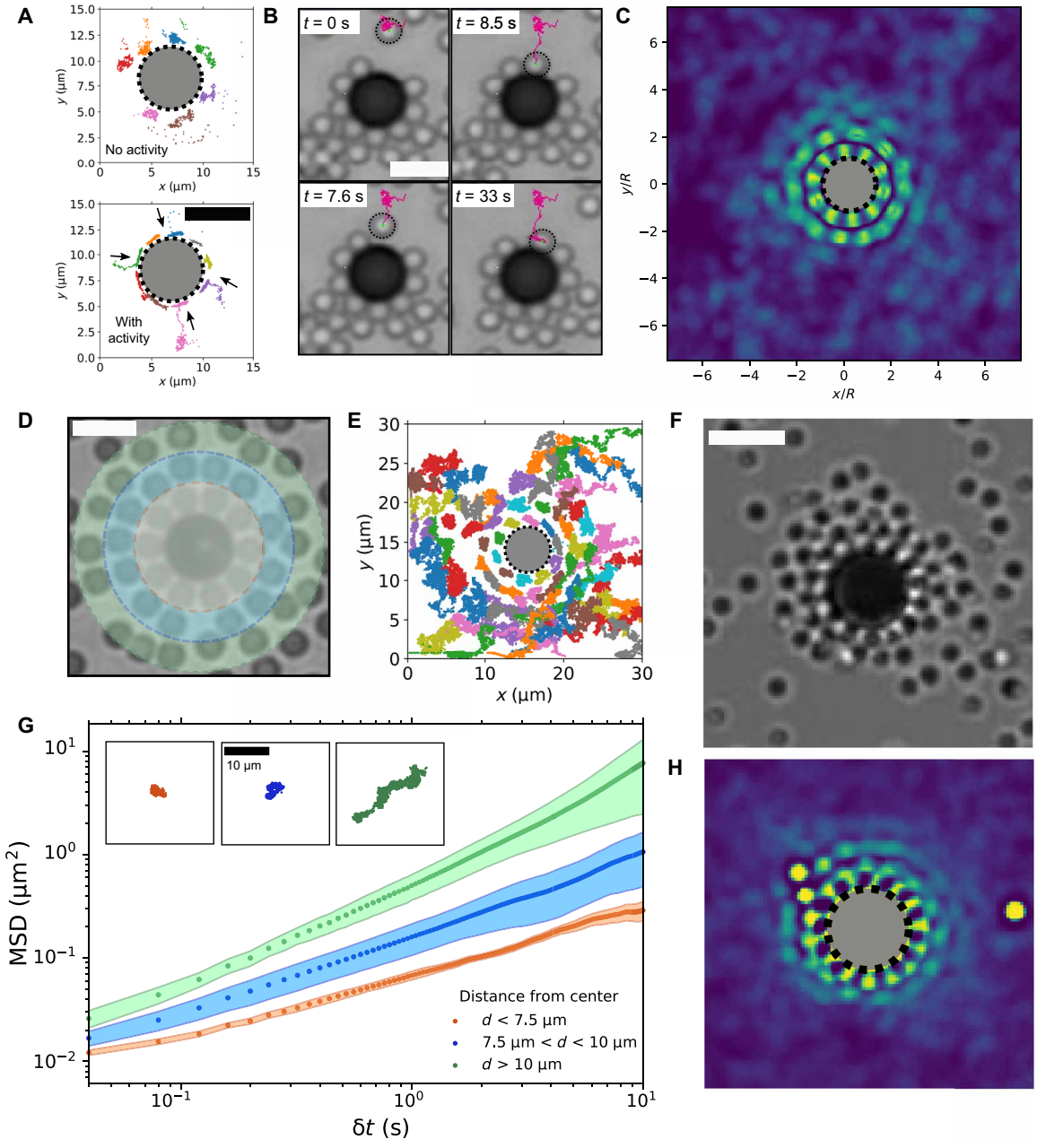

Fig. 1. Active-passive interaction for an immobilized Pt-silica Janus particle in an axis-perpendicular configuration. (**A**) Tracked trajectories of silica tracers (radius R_{tr} = 1 μm) near a Janus particle without (left) and with (right) H_2O_2. (**B**) Time-lapse images showing the attraction and retention of a tracer to an active Janus particle. (**C**) In-plane steady-state distribution of silica tracers (yellow regions) of radius R_{tr} = 1 μm around an active (6% H_2O_2) Janus particle (the gray disk at the center). (**D**) Snapshot showing multiple-rings accumulation of silica tracers around an active Janus particle; for reasons of visual clarity, a color overlay was added over each ring. (**E**) Tracked trajectories and (**F**) mean square displacement (MSD) of silica tracers starting from various locations around the center of the active particle. The insets in (F) show representative trajectories for each of the three classes of MSDs. (**G**) Snapshot showing the emergent multiple-rings structure for silica tracers of radius R_{tr} = 0.5 μm around an active Janus particle. (**H**) In-plane steady-state distribution of silica tracers (yellow regions) of radius R_{tr} = 0.5 μm around an active Janus particle (the gray disk at the center). The bright spot at the right edge is a spurious feature due to a tracer particle stuck at the wall. Except for (F), the scale bars correspond to 5 μm.

of tracer particles, emerges (see Fig. 2, A and C, and movie S3). Tracer particles, which are initially located in the vicinity of the Pt cap, are pushed away up to a distance of two to three *R* from the Pt cap. The repulsion in this region is sufficiently strong to overcome the diffusion of the tracer particles, which are subject to Brownian fluctuations, toward the Pt cap. The steady-state distributions shown in Fig. 2 (B and D) confirm these observations and reveal the formation of an exclusion zone, with a shape similar to that of a bean, behind the Pt cap (the deep blue region at the Pt side in Fig. 2, B and D).

It can be seen that—as for the case of the cap-perpendicular configuration—for the cap-parallel configuration, the behaviors exhibited by the tracers of different sizes are qualitatively the same

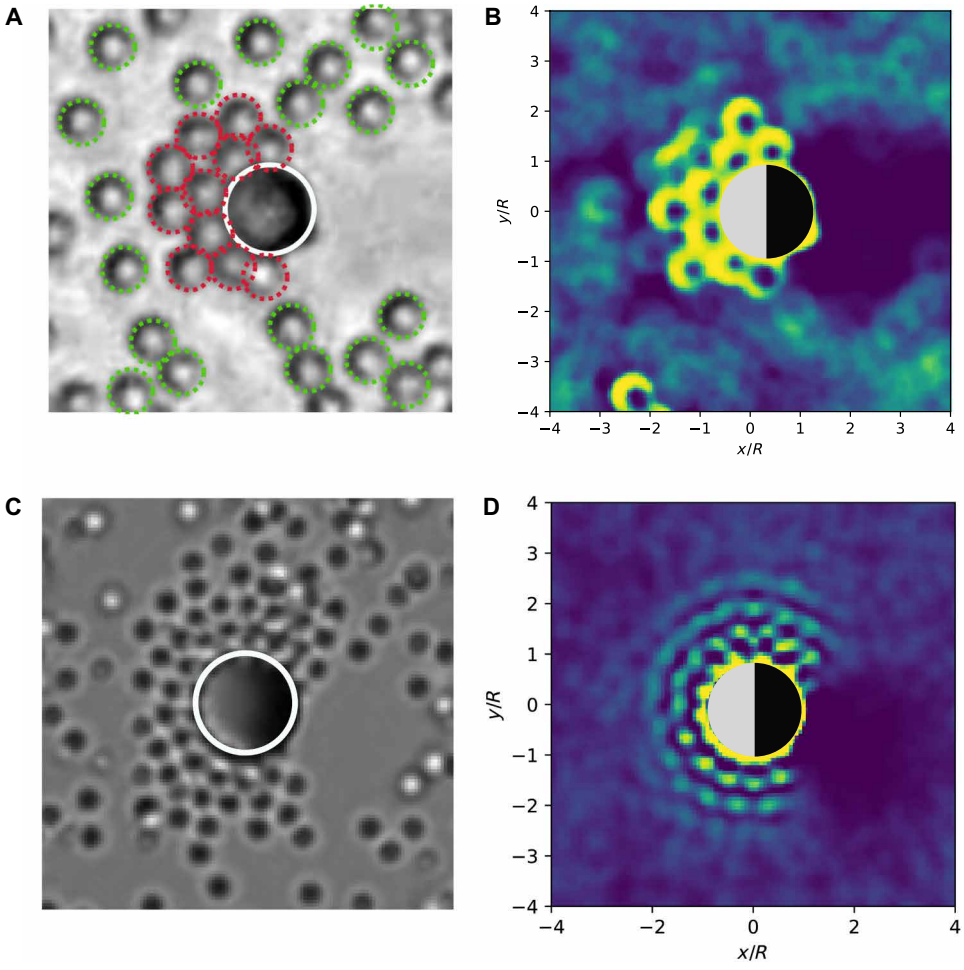

Fig. 2. Active-passive interaction for an immobilized Janus particle in an axis-parallel configuration. (**A** and **C**) Snapshots showing accumulation of silica tracers around an active (4% H_2O_2) Janus particle and formation of circular ring segments for tracers of radius R_{tr} = 1 (A) and 0.5 μm (C). (**B** and **D**) In-plane steady-state distribution of silica tracers around an active Janus particle in an axis-parallel configuration for tracers of radius R_{tr} = 1 (B) and 0.5 μm (D). The origin of the in-plane system of coordinates is set at the center of the active particle. The strongly attractive circular ring segment at the inert side of the Janus particle (the bright yellow at the left) is accompanied by the formation of a spatially extended zone completely depleted of tracers at the active, Pt-coated, side (deep blue region at the right).

(see movie S4). The only differences seem to be that a larger number of layers form in the compact semicircular region around the inert side for the smaller tracer size; however, the spatial extent of these layers is similar (approximately two to three *R*) for both tracer sizes.

Last, we note that both the number of rings of tracers formed on the silica side and the area of the depletion zone behind the active Pt side increase upon increasing the concentration of H_2O_2 fuel. It must also be emphasized that although the size of the depletion zone changes with fuel concentration, its shape does not.

Experiment: Motile (sliding state) Janus particle

We now consider the experimental observations in the case of motile active Janus particles, which move along the wall with their axes approximately within a plane parallel to the wall.

Dilute monolayer of tracers

The behavior of the tracers in the case in which the active Janus particle is motile, in a steady state of sliding along the wall, is more conveniently analyzed in a system of reference comoving with the particle (for details, see Methods). The origin of the comoving system is set to the center of the Janus colloid, the axes are chosen such that the *x*-*y* plane is parallel to the wall, and the direction *x* is parallel to the projection of the director **d** onto the wall.

As for the cases discussed in the previous subsections, the density of tracers (R_{tr} = 1 μm) was suitably adjusted to reach a compromise between keeping the system in the dilute monolayer limit while still having sufficiently many tracers around to allow a mapping of the characteristics of the active particle–tracer interactions during the time that the active particle is within the field of view of the microscope. The motile active particle can be seen to be in a wall-bound sliding steady state; although an accurate measurement of the orientation of the director **d** with respect to the wall is not possible, one can assess that **d** is quasi-parallel to the wall by noting that the visible dark area (Pt covered) represents approximately half of the disk area image of the Janus particle (Fig. 3A). [A detailed analysis of the mechanism leading to this stable cap–(quasi-)parallel configuration in motile active particles can be found in (*20*, *16*).]

The most notable feature is the absence of any ring structure at the silica side of the Janus particle, in contrast to the behavior observed when the Janus particle is stuck to the wall in the axis-parallel configuration. The trajectories evidence a tendency of the tracers

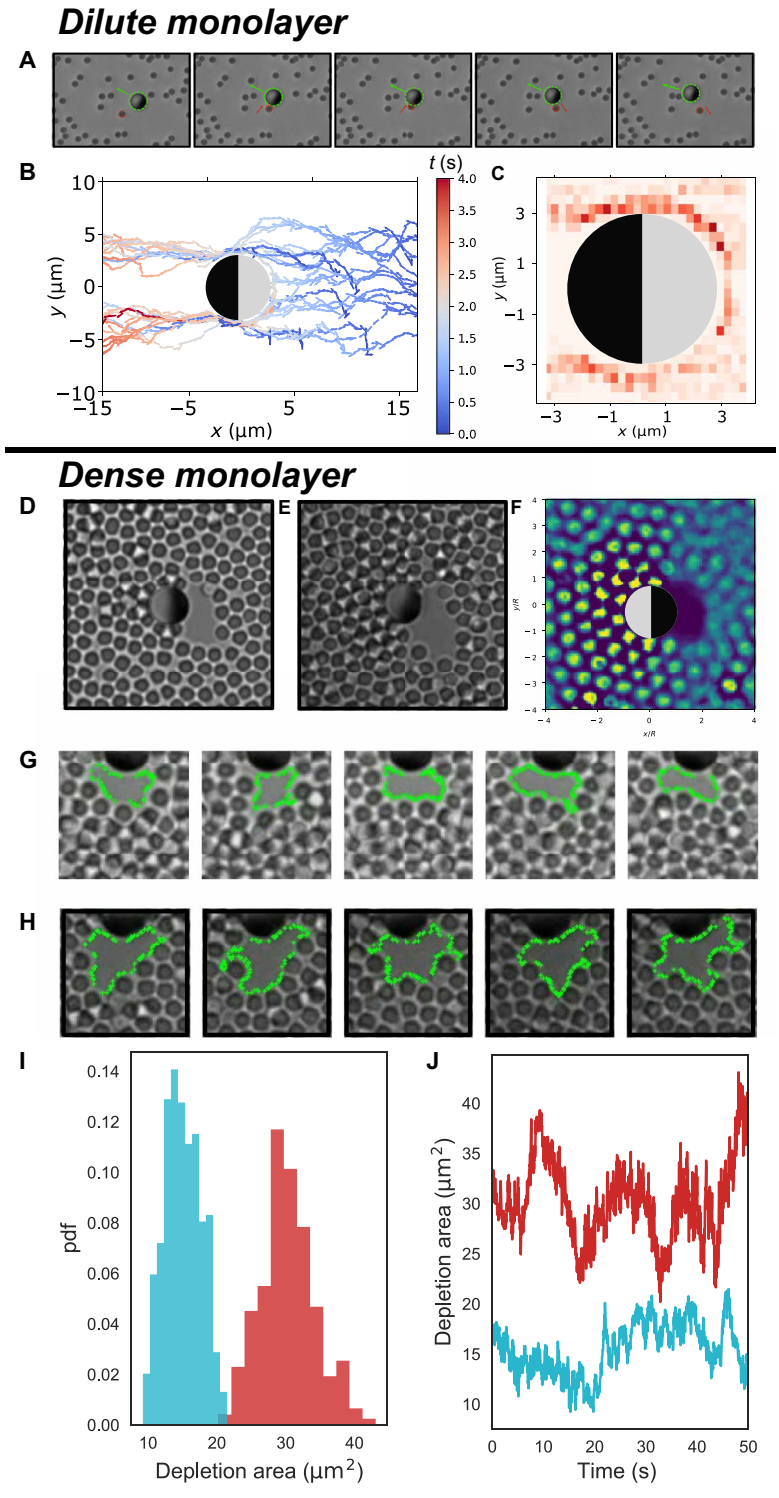

Fig. 3. Active-passive interactions for an active particle in an axis-parallel configuration in motile and jammed states. (**A**) Time-lapse images showing the interaction between a motile Janus particle (green) and a tracer (red). (**B**) Tracked trajectories (comoving frame of reference) of tracers interacting with a motile active particle. The color code depicts time progression from initial (deep blue) to final (deep red) state. (**C**) Two-dimensional histogram of contact points between the active particle and incoming tracers. (**D** and **E**) Depletion zone at the Pt cap of an active Janus particle jammed within a dense monolayer of tracers ($R_{tr} = 0.5$ μm), at 3 (D) and 6% (E) H_2O_2 concentration. (**F**) Steady-state probability distribution (pdf) of in-plane location of tracers around an active (3% H_2O_2) Janus particle in an axis-parallel configuration, in a jammed state: attraction (yellow spots) at the silica side and repulsion, i.e., depletion zone (the deep blue region at the right), at the Pt side. (**G** and **H**) Illustration of the automated tracking of shape and area of the depletion zone; the snapshots are separated by 6 s. (**I**) Histogram and (**J**) time dependence of the area of the depletion zone for H_2O_2 concentrations of 3 (cyan) and 6% (red).

located in the proximity of the active particle to be drawn in toward the equator region, as well as a clear repulsion at the Pt side (Fig. 3B and movie S5). The tracers colliding head-on with the active particle slide along the silica cap until reaching a point just past ($\lesssim$1 μm) the equator, after which they are repelled (see the kinks in the trajectories in Fig. 3B at the point of leaving the surface of the Janus particle). From this image sequence, it is also possible to extract the probability of finding a tracer at a certain location along the surface of the Janus particle, which is shown in Fig. 3C. This "heatmap" confirms an increased probability of contact in a region near the equator that extends from the silica side by ≈1 μm into the Pt side, i.e., in the region where the passive particles are actively drawn in (see Fig. 3A). Furthermore, the heatmap clearly documents the lack of any contact with tracers on the central part of the Pt side, i.e., this is a region of substantial effective repulsion experienced by the tracers.

Dense monolayer of tracers: Motile Janus particle in a jammed state

Last, we have also studied the case in which a motile Janus particle is trapped in a jammed state inside a dense (quasi–close-packed) monolayer of tracers of radii R_{tr} = 1 μm (see Fig. 3); i.e., although the active particle is, in principle, motile (not stuck to the wall), it reaches a stall state, the stall force being provided by the pressure in the monolayer of tracers. (The inert particles are thus no longer just tracers for the fields sourced by the active Janus particle; they directly interact with the active particle and influence its dynamics.) To ensure this setup, we have restricted the study only to the Janus particles (within the dense silica particle monolayer) that, upon addition of H_2O_2, visibly change their orientation to being axis parallel. This is indicative of them being potentially motile, albeit unable to move because of being jammed within the densely packed monolayer. Although this setup is conceptually much more difficult to approach and analyze theoretically (a task which we leave for future work), we briefly discuss it below.

Once the Janus particle is active, one observes a reorganization of the monolayer, with the emergence of a depletion zone at the Pt side of the particle and a ring-structured compression region at the silica side of the particle (see Fig. 3, D and E, and movie S6). By analyzing the time-averaged distribution of tracers around the jammed Janus particle, two- to three-ordered ring segments are apparent at the inert (silica) side (the bright yellow spots in Fig. 3F). In contrast, the depletion zone at the Pt side of the active particles (the deep blue zone in Fig. 3F) is fluid, with substantial changes in shape over time as the surrounding tracers try to diffuse into this area (Fig. 3, G and H). Despite the changes in shape, the area of the depletion zone fluctuates around a well-defined average value (see Fig. 3J); this value depends on the H_2O_2 concentration, and it increases upon increasing the H_2O_2 concentration (Fig. 3, I and J), which clearly argues that the emergence of the depletion zone is a result of the chemical activity of the jammed Janus particle.

Theoretical interpretation of the behavior of tracers near an immobilized active Janus particle

It is evident that a system of catalytically active Janus particles in a bath of inert tracers exhibits a very rich behavior that depends on the orientation and state of motion of the Janus particles. Intrinsically, this behavior emerges from a complex interplay of chemical and hydrodynamic effects. First of all, active Janus particles achieve self-propulsion through an interfacial coupling between self-generated chemical and hydrodynamic fields. Specifically, the chemical gradients that arise from the reaction on the catalytic "face" of the particle, in combination with (material-dependent) molecular forces between the particle surface and the various molecules in the solution, lead to so-called self-phoretic motion (*32*, *33*). The chemical and flow fields implicated in the self-phoretic motion of a Janus particle are affected by geometric confinement, i.e., by the presence of the hard planar wall beneath the Janus particle (*16*) (as well as, in general, by the presence of other particles). Second, the inert tracers respond both to local chemical gradients (via phoresis) and to flow; their motion is the net result of these contributions. Third, the same interfacial mechanism that couples chemical gradients and flow in the vicinity of the surface of a Janus particle can also take place on the planar wall, i.e., chemiosmosis can occur (*30*). In addition, we note that if the catalytic reaction involves charged intermediates, then there may be electric fields in the solution leading to electrophoretic contributions to the motion of the Janus and/or tracer particles (*34*). Unraveling the interplay of these effects is a challenging task.

Here, our aim is to develop a minimalistic, coarse-grained model that has few adjustable parameters, and which yet still captures the main qualitative features observed in the experiments. To simplify this task, we focus on the case of immobilized Janus particles in a dilute bath of tracers. To interpret and rationalize the experimental observations, we consider a previously used simple continuum model of chemical gradients and hydrodynamic flow created by an immobile, catalytically active Janus particle near a planar wall (see Methods) (*16*, *20*, *30*, *31*). In brief, at the catalytic cap of the particle, solute molecules (i.e., oxygen) are released in the solution. The connection between the gradients of the solute number density $c(\mathbf{x})$ (chemical field), where $\mathbf{x}$ is a position in the solution, and the hydrodynamic flow $\mathbf{u}(\mathbf{x})$ of the solution is assumed to be that of a slip velocity as in the classical theory of neutral diffusiophoresis (*32*, *33*). Accordingly, each surface is characterized by a certain so-called phoretic mobility (or surface mobility) coefficient: b_w at the wall, b_c at the catalytic cap, and b_i at the inert part of the Janus particle. These coefficients encode the material-dependent interactions between the solid surfaces and molecules in the solution. We note that our coarse-grained model does not resolve charged intermediates or electric fields.

We consider the motion of a single tracer; this is analyzed in the point-particle limit, i.e., the tracer responds to the chemical gradients and hydrodynamic flow created by the particle and the wall, but only weakly and locally disturbs these fields. Accordingly, the tracer particle is advected by the hydrodynamic flow with velocity $\mathbf{u}(\mathbf{x}_t)$ [where $\mathbf{x}_t = (x_t, y_t, z_t)$ denotes the location of the center of the tracer] and responds to chemical gradients via phoresis (*32*), i.e., it drifts with a phoretic velocity $b_t\nabla c(\mathbf{x}_t)$, where b_t is the phoretic mobility of the tracer. Furthermore, we can distinguish advection by the chemiphoretically driven flow $\mathbf{u}_p(\mathbf{x}_t)$, originating at the surface of the Janus particle, and advection by the chemiosmotically driven flow $\mathbf{u}_w(\mathbf{x}_t)$, originating at the wall. We thus write

$$\mathbf{v}_t(\mathbf{x}_t) = \mathbf{u}_p(\mathbf{x}_t) + \mathbf{u}_w(\mathbf{x}_t) + b_t\nabla c(\mathbf{x}_t) \quad (1)$$

where $\mathbf{v}_t(\mathbf{x}_t)$ is the velocity of the tracer particle as a function of its position $\mathbf{x}_t$. We note that if $\mathbf{v}_t$ has a component directed toward the center of the Janus particle, then the tracer has an effective attractive interaction with the Janus particle when the tracer is at $\mathbf{x}_t$; likewise, if $\mathbf{v}_t$ has a component directed away from the center of the Janus particle, then the tracer has an effective repulsive interaction with the Janus particle at $\mathbf{x}_t$.

In the following calculations, we assume that the tracer particle has sedimented to the vicinity of the wall and (because of its appreciable weight) maintains only in-plane mobility; this is consistent with the experimental observation that the tracers always remain in focus when viewed with optical microscopy. The distance from the surface of the tracer to the wall (separation) is expected to be in the range of tens of nanometers. This parameter is expected to have only a weak influence on the phenomenology, as long as the height of the center of the tracer to the wall is taken to be slightly larger than the radius of the tracers. In units of the radius R of the Janus particle, the tracer particles have radii $R_{tr} = 0.4R$ or $R_{tr} = 0.2R$, respectively; in this work, we take the height $h_{tr} := z_t/R$ of the center of the tracer particle to be $h_{tr} = 0.41$ or $h_{tr} = 0.21$ for the larger and for the smaller tracers, respectively. In what concerns the stuck Janus particle, we will model it as being stalled, by suitable external force and torque, in the particular configuration of interest (axis perpendicular or axis parallel) and slightly above the surface, rather than being in direct contact with the wall; i.e., the center of the Janus particle is taken to be located at $h/R = 1.1$, rather than being in direct contact with the wall. This vertical shift and its value (as long as not too large) are expected to not influence the qualitative features of the emergent dynamics (see also Methods); however, it notably reduces the technical, numerical difficulties in determining the chemical field and the hydrodynamic flow.

Noting that the magnitude of one of the phoretic mobilities, e.g., $|b_c|$, can be absorbed in the definition of a velocity scale (*33*) U_0 (see Methods), the model depends on four parameters: the sign of b_c and the mobilities b_i, b_t, and b_w. The special choice of materials used in the current experiments, in which the tracers and the inert part of the Janus particle are made from the same material (silica), implies the expectation that $b_t \simeq b_i$. From general considerations on the direction of motion of these Janus particles when far from the boundaries and on their rotations when in the vicinity of walls (see note S4), it is inferred that b_c is negative and it is expected that $0 \leq \beta_i := b_i/b_c < 1$. Accordingly, the number of parameters is reduced to two, which we chose to be β_i and $\beta_w := b_w/b_c$. Furthermore, by noting that the wall is made of glass (another form of silica), it is reasonable to expect that b_w and b_i have the same sign and $|b_w| \sim |b_i|$ (thus $\beta_w \sim \beta_i$).

Before proceeding with the analysis, we note the following aspects concerning the various terms in the right-hand side of Eq. 1. Owing to $\beta_t > 0$, because $\beta_t := b_t/b_c = \beta_i$, the phoretic component of the motion of the tracers (the last term in Eq. 1) corresponds to an effective repulsion (motion away from the source of chemical, i.e., away from the Janus particle). Consequently, agreement with the experimental observation of tracers accumulating in the vicinity of the active Janus particle can be achieved only if the in-plane ($z_t/R = h_{tr}$) drift by the hydrodynamic flow $\mathbf{u}_p + \mathbf{u}_w$ is toward the Janus particle and of sufficiently large magnitude. For a wall with osmotic slip, for $b_w < 0$ (as it is expected for our system), the contribution $\mathbf{u}_w$ to the motion of the tracer is always oriented toward a Janus particle in a cap-perpendicular configuration, irrespective of that being cap-up or cap-down; i.e., in this configuration, the osmotic-driven flow $\mathbf{u}_w$ is providing an effective attraction component to the motion of the tracer.

The discussion above leads to the expectation that for the system of silica tracers near a silica/Pt Janus particle immobilized at a glass wall, the parameters β_w and β_i have similar values. Accordingly, we focus below on the case $\beta_w = \beta_i$ and study the behavior of the tracer as a function of the parameter $\beta_i (= \beta_t = \beta_w)$. As shown below, for this choice there exist values β_i for which the theoretically predicted effective interactions experienced by the tracers are compatible with the experimental observations. The alternative scenario that the two parameters take very different values cannot be ruled out a priori (but, anticipating, we have shown that it does lead to theoretical predictions in disagreement with the experimental observations). Accordingly, the discussion is complemented, in note S2, by an analysis of the case of a no-slip wall ($\beta_w = 0$), representative for a situation with $|\beta_w| \ll |\beta_i|$. For completeness, in note S3, we also succinctly discuss, focused on the axis-perpendicular configuration, the case opposite to a no-slip wall; i.e., the case in which the response to the chemical gradients at the wall is much stronger ($|\beta_w| \gg |\beta_i|$) than at the inert part of the Janus particle.

Axis-perpendicular configuration

A Janus particle stuck with its director perpendicular to the wall provides a configuration with axial symmetry (see Figs. 4 and 5), which is amenable to analytical treatment. The solutions $c(\mathbf{x})$ and $\mathbf{u}(\mathbf{x})$ for the Laplace and Stokes problems defined above can be written in terms of series in bipolar coordinates by using the classical results from (*35*, *36*), adapted to account for the phoretic slip at the surface of the particle and at the wall as in, e.g., (*37*). (These series solutions do not provide much physical insight, and thus, we do not list them here; the interested reader can consult the references noted above.)

As noted in the discussion of the experimental results, the optical microscopy cannot discriminate between cap-up and cap-down orientations. However, it turns out that, for a cap-down configuration, there is no combination of parameters β_w and β_i for which the experimental observations can be reproduced by the theoretical model, as shown below for the case $\beta_w = \beta_i$ and—as noted above—in the Supplementary Materials for the case $\beta_w \neq \beta_i$ (see note S1). For reasons of brevity, we present here only the results in the case of the tracers of radius 1 μm because this is sufficient to rule out the cap-down configuration. [Nonetheless, we note that, for the smaller tracers (radius, 0.5 μm), the results are basically the same, with the only difference being in the somewhat smaller values of the corresponding Péclet numbers.] Figure 4 illustrates typical results for the solute density, hydrodynamic flow, and tracer flow (as well as the tracer Pe_t number) corresponding to this case. It is seen that, at all values $0 < \beta_i < 1$, the tracers exhibit a repulsive effective interaction (see the tracer flows in the right column). Furthermore, the Péclet number of the tracers, shown by the background color in right column panels in Fig. 4, is very large ($Pe_t \gg 1$) even at large distances $\Delta \simeq 4R$ from the center of the Janus particle; i.e., in this case, the prediction is also a basically deterministic outward motion (contrary to the experimental findings of attraction toward the active particle). Accordingly, the cap-down configuration can be ruled out, in that there is no combination of parameters for which the theoretical predictions can be reconciled with the experimental observations.

We turn now to the case of a cap-up configuration, and we study it for various values of the parameter $0 \leq \beta_i (= \beta_w) < 1$. (We remind that the analysis of the case $\beta_i \neq \beta_w$ is provided in notes S2 and S3.). For the cap-up configuration, the contribution from the wall-driven flows qualitatively influences the behavior exhibited by the tracers, as shown in Fig. 5 (for the tracers of radius $R_{tr} = 0.5$ μm and $R_{tr} = 1.0$ μm). When the osmotic slip is accounted for, the effective interaction exhibited by the tracers is attractive near the colloid and weakly repulsive very far from the colloid. The extent of the region where the effective interaction is attractive increases upon decreasing

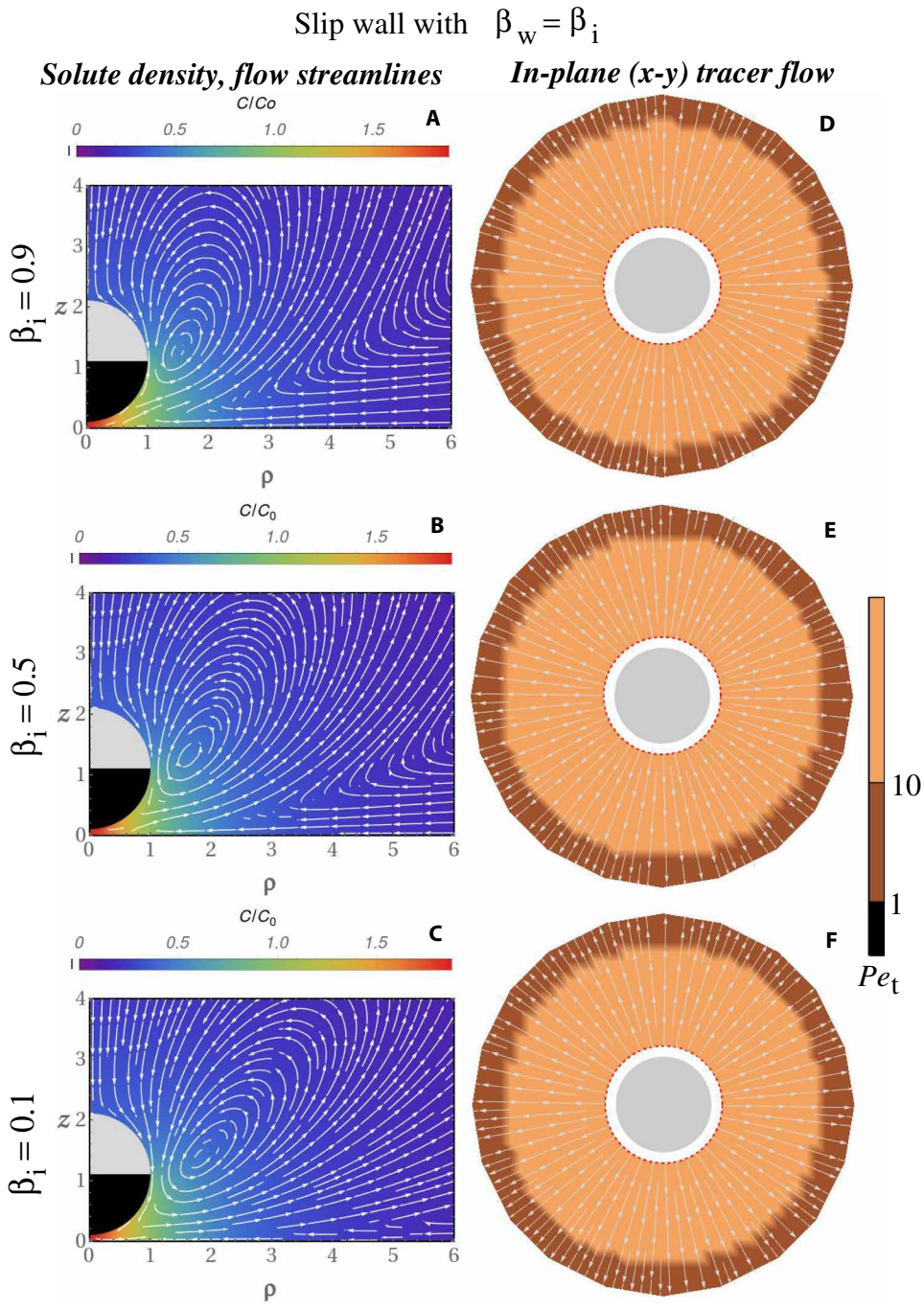

Fig. 4. Chemical field, hydrodynamic flow, and the emergent tracer dynamics around an immobile active Janus particle in a cap-down configuration near a wall with phoretic mobility coefficient $b_w = b_i$. Left column (**A** to **C**): Dimensionless solute density (color-coded) and hydrodynamic flow streamlines corresponding to the immobile silica/Pt Janus particle located at $h/R = 1.1$. Right column (**D** to **F**): *x*-*y* in-plane flow response of large ($R_{tr} = 1.0\,\mu m$, $h_{tr} = 0.41$) silica tracers ($b_t = b_i$) to the activity of the Janus particles (gray disks, as viewed from above). The color-coded background shows the corresponding Pe_t values. The corresponding values β_i are indicted at the left of each row. Red circles indicate the in-plane exclusion zone (of radii ~1.2*R*), which is due to the tracer–Janus particle hard-core interaction.

β_i (compare the top and middle panels in the middle and right columns of Fig. 5). The Péclet number of the tracers, $Pe_t = |\mathbf{v}_t| R_{tr}/D_{tr}$, which is shown color-coded in the panels in the middle and right columns of Fig. 5, provides additional insight into the behavior. [Note that throughout the following analysis, we account for the hindrance of the tracer diffusion by the wall, using the assumed tracer height (*38*)]. For the smaller tracers, it is only for $\beta_i < 0.5$, and particularly $\beta_i \lesssim 0.2$, that regions of attractive interactions where the Péclet numbers are large (therefore, the deterministic biased motion toward the active particle dominates the Brownian motion) occur near the Janus particle. Similarly, for the larger tracers, for $\beta_i \lesssim 0.5$, there are regions of attractive interactions, starting from the point

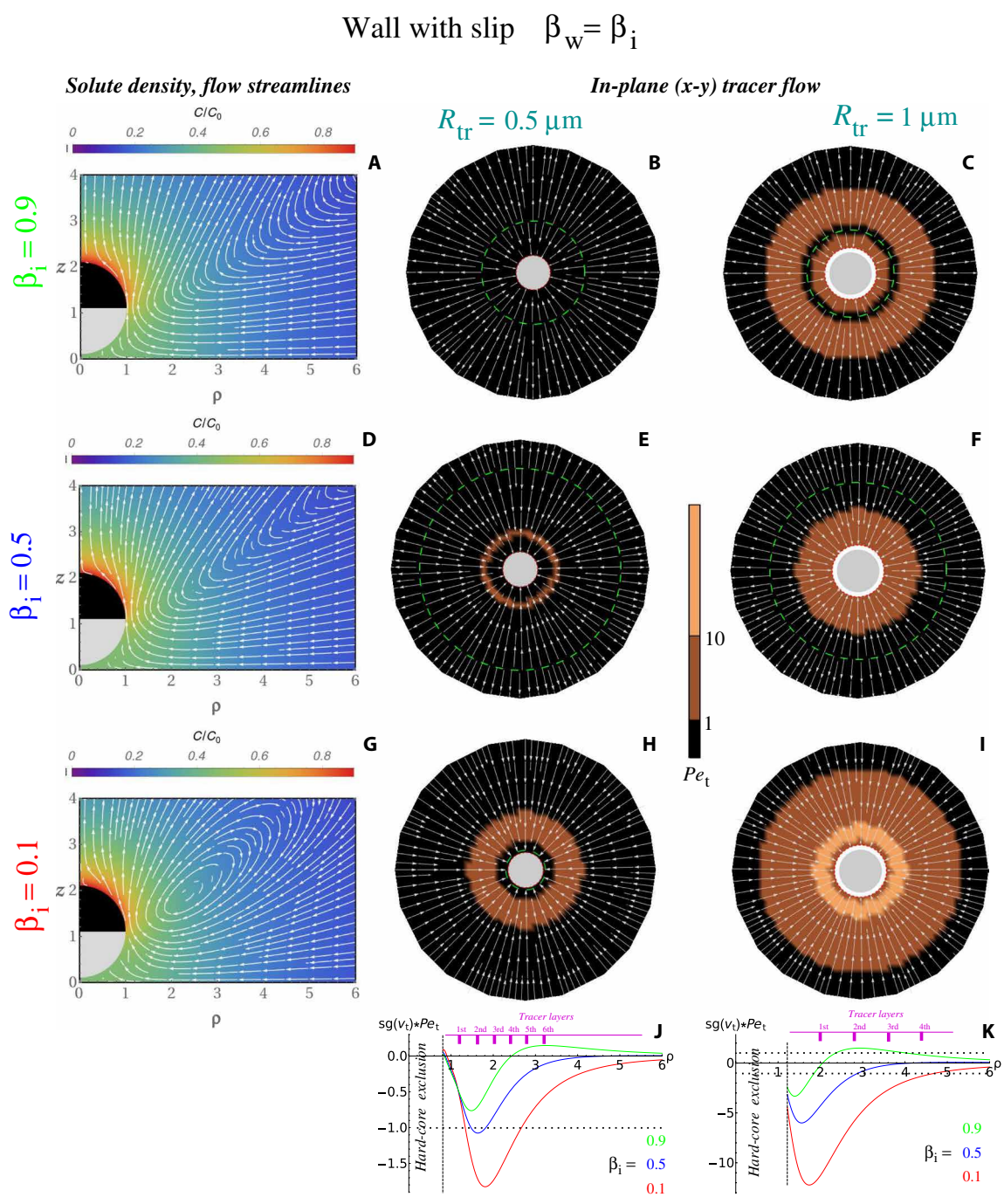

Fig. 5. Chemical field, hydrodynamic flow, and the emergent tracer dynamics around an immobile active Janus particle in a cap-up configuration near a wall with phoretic mobility coefficient $b_w = b_i$. (**A** to **C**) Dimensionless solute density (color-coded) and hydrodynamic flow streamlines corresponding to the immobile silica/Pt Janus particle located at $h/R = 1.1$. (**D** to **I**) $x - y$ in-plane flow response of (D to F) small ($R_{tr} = 0.5$ µm, $h_{tr} = 0.21$) and (G to I) large ($R_{tr} = 1.0$ µm, $h_{tr} = 0.41$) silica tracers ($b_t = b_i$) to the activity of the Janus particles (gray disks, as viewed from above). The color-coded background shows the corresponding Pe_t values. The corresponding values β_i are indicted at the left of each row. Red circles (D to I) indicate the in-plane exclusion zone, which is due to the tracer–Janus particle hard-core interaction. Green dashed circles in (B), (C), (E), and (F) mark the location at which the motion of the tracers changes direction: toward (away from) the Janus particle if the tracer is inside (outside) this domain. Bottom row (**J** and **K**): Signed Péclet number versus radial distance for the small (J) and large (K) tracers, for the three values $\beta_i = 0.1$, 0.5, and 0.9. The dotted lines indicate the values sg(v_t) $Pe_t = \pm 1$. The magenta markers and numbers indicate the ends of close-packed tracer layers (rings).

of steric contact with the Janus particle, where the Péclet numbers are large (i.e., $Pe_t \gg 1$). For $\beta_i \lesssim 0.2$ for the smaller tracers, and for $\beta_i \lesssim 0.5$ for the larger tracers, the spatial extent Δ (measured from the center of the active particle) of the region with attractive interactions and $Pe_t > 1$ is in the range of three to five R (compare the red curve with the blue and green ones in Fig. 5J and the red and blue curves with the green one in Fig. 5K). These features are compatible with the experimental observations (discussed in the previous subsections)

of concentric rings, with compact structure near the colloid (stronger attraction, large Pe_t), followed by a sparse structure toward the outer ring ($Pe_t \gtrsim 1$) merging into Brownian motion ($Pe_t < 1$) at larger distances.

In summary, the analysis for the axis-perpendicular configurations implies first that the configuration with the axis perpendicular to the wall observed in the experiments is the one of cap-up orientation (see also note S1), and second that agreement between the theoretical predictions and the experimental observations requires that the wall is responsive (via the osmotic slip) to the chemical activity and that this response is relatively weak (i.e., $\beta_w = \beta_i \lesssim 0.2 - 0.3$).

The requirement of wall responsiveness can be further tested by analyzing walls with different β_w. Because β_w is a material property of the surface, different values of β_w can be accessed by changing the material type of the bottom wall that is used in the experiments. We expect that, if the osmotic response at the wall is a relevant parameter for these systems, then different surfaces should lead to different levels of attraction or repulsion of the tracer particles to the active particle. We perform experiments similar to the ones described in the previous section, using the same active particles (silica-Pt) and tracers (silica, $R_{tr} = 1$ μm), but using different wall surfaces made of glass, mica, and Ti. (For the case of Ti, a 25 nm layer of Ti is sputter-coated onto a plain glass slide.) In each case, we study the response of tracers near Janus particles stuck at the wall in an axis-perpendicular configuration. We ensure that the level of activity in systems with different walls remains the same by using the same batch of active particles (fabrication processes sometimes cause variations in the activity of the particles) and the same concentration of H_2O_2 (3%, v/v). For all three surfaces, we observe that, upon addition of H_2O_2, the tracers in the vicinity of active particles are drawn in toward the active particle (see Fig. 6A). However, the magnitude and the spatial extent of this attraction clearly vary by surface type. For the case of a glass surface, we find that two strongly bound rings form around the active particle, and an additional weakly bound ring persists. For the case of a Ti surface, we only observe a single strongly bound ring and an additional weakly bound ring. The attraction on the mica surface is the weakest: Only a single weakly bound ring forms around the active particle. The difference in the level of attraction on the different surfaces is clearly visible in the probability densities of tracer positions in proximity of the active particles (see Fig. 6B).

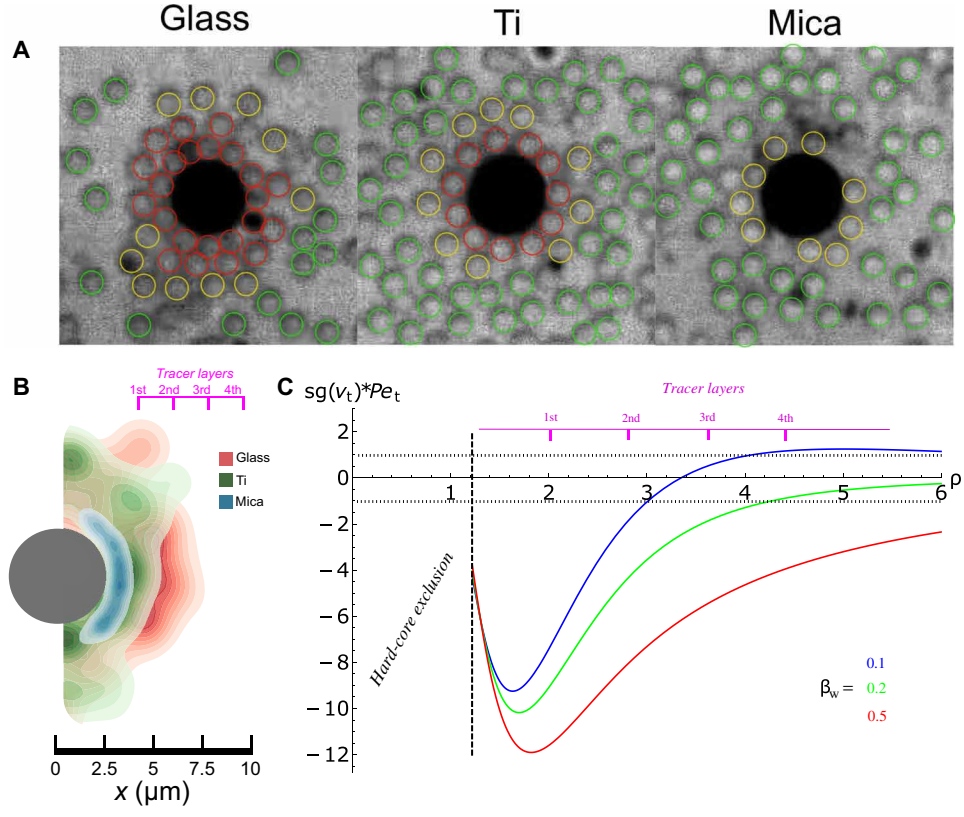

Fig. 6. Active-passive interaction for an immobilized Janus particle in an axis-parallel configuration for different surface types. (**A**) Snapshots showing accumulation of silica tracers around an active Janus particle and formation of circular ring segments for tracers of radius $R_{tr} = 1$ μm for different surface types (glass, Ti, and mica). The tracers indicated in red are tightly bound to the active particle, tracers in yellow are weakly bound to the active particle, and the tracers in green are unbound in the solution. (**B**) Probability density of the silica tracer particles ($R_{tr} = 1$ μm) accumulated near the active Janus particle on the three different surface types (glass, Ti, and mica). The magenta markers indicate the ends of close packed tracer layers (rings). Color code: Deep color corresponds to high probability, white to the "far" constant value (inverse of the average tracer density). (**C**) Signed Péclet number for a tracer with $z_{tr}/R = 0.41$ in the vicinity of a cap-up Janus particle with $\beta_t = \beta_i = 0.2$. Negative values of $sg(v_t)\ Pe_t$ indicate radial attraction. Roughly speaking, the effective attraction dominates the Brownian motion when $sg(v_t)\ Pe_t < -1$, and this condition is used to define the extent of the region of effective attraction. The various curves correspond to different values of the wall phoretic mobility ratio β_w, such as would be obtained with different substrate materials. The dotted lines indicate the values $sg(v_t)\ Pe_t = \pm 1$. The magenta markers and numbers indicate the ends of close-packed tracer layers (rings).

Qualitatively, this dependence on the material composition of the wall can be recovered in the theoretical model. Specifically, we fix $\beta_t = \beta_i = 0.2$ (consistent with the range inferred from the analysis summarized in Fig. 5) to represent the fact that silica tracer particles and Pt/silica Janus particles were used throughout this series of experiments. We consider various values of the wall phoretic mobility ratio β_w for an $R_{tr} = 1$ μm tracer ($z_t/R = 0.41$), as shown in Fig. 6C. Using the simple criterion that the biased motion (here attractive, $v_t < 0$) prevails over Brownian motion when $Pe_t > 1$, i.e., the signed Péclet number $\mathrm{sg}(v_t)\, Pe_t < -1$, we find that the extent of the region of attraction (i.e., the region in which the $\mathrm{sg}(v_t)\, Pe_t$ curve corresponding to a certain value β_w takes values smaller than −1) increases with β_w. Thus, by comparison with the trend observed in the experiments, we infer that $\beta_{w,\,mica} < \beta_{w,\,Ti} < \beta_{w,\,silica}$, where here we assume that $\beta_{w,\,silica} \approx 0.2$. While quantitative agreement with the experiments (in terms of number of bound rings) may be possible upon tuning β_t within $0 < \beta_t < 0.3$, we do not further pursue this aspect because these findings would have limited significance, considering the simplicity of the model used, the dilute tracer approximation, the somewhat ad hoc (although being a reasonable choice) character of the $\mathrm{sg}(v_t)\, Pe_t < -1$ criterion for estimating the spatial extent of layering, etc. Overall, the experiments and modeling converge to the conclusion that the material composition of the substrate has a profound influence on tracer dynamics and that this dependence can be rationalized as being due to the material dependence of the chemiosmotic slip.

A further brief comment concerning the conclusion of a cap-up orientation is in order. As noted in the discussion of the experimental results shown in Fig. 1, upon drying out of the suspension with Janus particles, one observes particles adhered to the glass slide in various orientations, with no obvious preference between a cap-down and a cap-up configuration (see also note S5). We think that the reason why only the latter persists once the chemical activity of the particles is turned on is the following. In the cap-down configuration, the moving up tendency of the active particle is strongly enhanced by the confinement, due to the wall, of the chemical field and can overcome the adhesion produced by the surface [via Derjaguin-Landau-Verwey-Overbeek (DLVO) forces]. In contrast, in the cap-up configuration, the tendency of the particle is to move into the wall, and thus, it cooperates with the surface interactions; in addition, in this configuration, the chemical field is only weakly affected by the wall confinement. Visual observations of events of detachment of Janus particle from the wall, followed by a fast turn to a sliding state, seem to better match with the picture of a rotation from a cap-down initial state than with one from a cap-up initial state.

Axis-parallel configuration

Now, we consider the theoretical results for an immobile Janus particle in a cap-parallel configuration. The low symmetry of this configuration requires a numerical approach to obtain the concentration and flow fields, and we use the boundary element method (see also Methods).

For the case of an osmotic-responsive wall with $b_w = b_i$, we explored the behavior exhibited by the tracers in the vicinity of the Janus particle for $0 \le \beta_i \le 1$. The results are summarized in Fig. 7 for the small ($R_{tr} = 0.5$ μm) tracers and in Fig. 8 for the larger ($R_{tr} = 1$ μm) tracers. For $\beta_i = 0.3$, tracer particles are attracted to most of the inert face of the particle, with the exception of two regions near the equator of the particle. As β_i is increased above $\beta_i = 0.3$, the angular extent of the attraction is increasingly restricted to the inert pole (not shown). Consequently, one concludes that $\beta_i \le 0.3$ is seemingly required to achieve qualitative agreement with the experimental results, which show a first ring of tracers occupying the entire circumference at the inert side and the next partial rings being located within a cone-like region extending from the equator of the Janus particle (see Fig. 2 and the discussion there). Both $\beta_i = 0.1$ and $\beta_i = 0.2$ show good agreement with the experimental observations. Specifically, the results imply that tracer particles will collect around the entire inert face of the particle and even extend slightly past the equator. Furthermore, the number of layers of tracers will have the expected cone-like structure, i.e., fewer layers will collect at the inert pole than closer to the equator. As a point of disagreement between theory and experiment, we note that, in the experiments, the region of collected particles extends notably beyond the equator in Fig. 2 (C and D). To some extent, this discrepancy may be due to steric interactions between tracers: Tracers in the side vortices may have their motion hindered by layers of tracers collected around the inert cap and remain trapped there. For the large tracers ($R_{tr} = 1$ μm), we obtain similar phenomenology (Fig. 8), including the restriction of the angular region of attraction as β_i is increased above $\beta_i = 0.3$. However, for the large tracers, the region of effective attraction ($Pe > 1$) has a longer range. While the complex topology of the tracer pathlines provides the best point of comparison with the experiments, we also comment here on the extent of region that has $Pe_t > 1$ and inward motion of tracers. For the small tracers, this region extends two tracer diameters from the inert pole and three diameters from the equator, which is in reasonable agreement with the number of layers in Fig. 2. For the large tracers, this region has a width of several diameters, which is somewhat more than is observed in Fig. 2.

From these results, one concludes that if the wall and the inert face have the same surface mobilities, then the parameter β_i is constrained as $0 \le \beta_i \le 0.3$. In other words, differences between theory and experiment diverge sharply as β_i increases beyond $\beta_i \simeq 0.2$ to 0.3. Most notably, for $\beta_i \ge 0.4$, the angular region of the inert face that attracts particles is restricted to 90° or less, instead of the entire 180°. (The value $\beta_i = 0.3$ has no special significance in itself, but we find that it is the largest value of β_i showing any plausible agreement with the experimental observations.)

Last, we comment on the effect of the wall on the tracer behavior for an active immobile particle in an axis-parallel configuration [i.e., for either $b_w = 0$ (see note S2) or $b_w = b_i$] via a comparison with the case of an immobile particle far from boundaries (see fig. S8 in note S4). In the presence of a wall, and for values of the parameters for which the theoretical predictions are compatible with the experimental observations (i.e., $0 \le \beta_i \le 0.3$), there is a recirculating region of tracer flow near the equator that acts as a barrier preventing diffusion of a tracer particle from the region of attraction surrounding the inert face to the region of repulsion surrounding the catalytic face. Therefore, a stuck tracer particle is very unlikely to diffuse around the rim of the Janus particle from the inert face to the catalytic face and leave the Janus particle, a prediction which is in agreement with experimental observations. For the immobile particle far from boundaries, there are some tracer pathlines that terminate on the excluded volume region (see fig. S8). In particular, there is a stagnation point for the tracer flow on the inert pole for all β_i. However, on both sides of the stagnation point, we see that either the tracer pathlines tend to carry the particle around the rim, toward the equator, or there is no barrier to diffusion around the rim, i.e., the pathlines (which, recall, sum the effects of tracer phoresis and advection by hydrodynamic flows) do not oppose diffusion of the

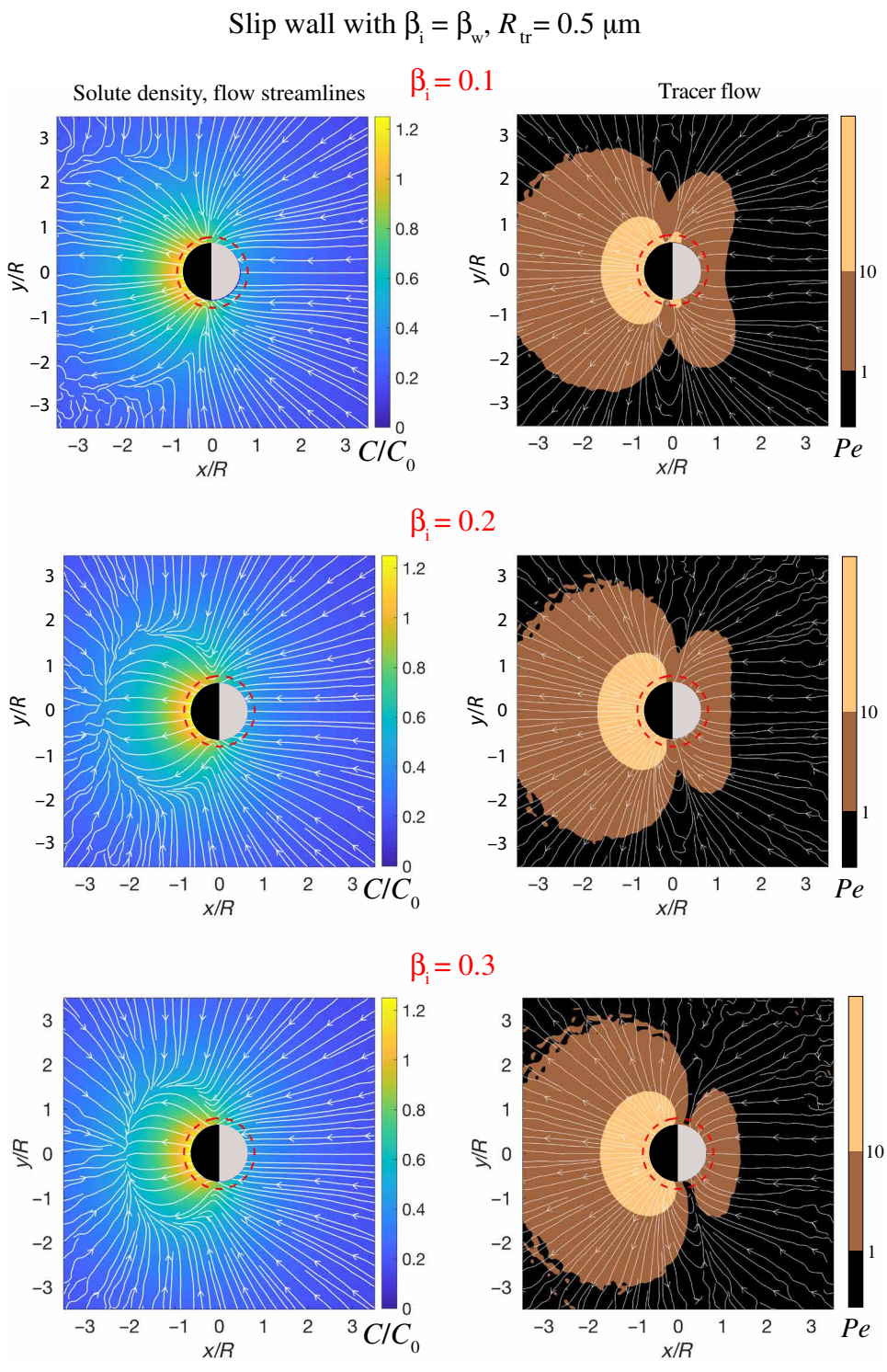

Fig. 7. Chemical field, hydrodynamic flow, and the emergent tracer dynamics around an immobile active Janus particle in a cap-parallel configuration near a wall with phoretic mobility coefficient $b_w = b_i$ for tracer size R_{tr} = 0.5 μm. Left column: $x - y$ in-plane ($z_t/R = h_{tr} = 0.21$) and dimensionless (in units of $c_0 := \kappa R/D$) solute density (color-coded) and hydrodynamic flow streamlines corresponding to the immobile silica/Pt Janus particle located at $h/R = 1.1$. **Right column:** x-y in-plane ($z_t/R = h_{tr} = 0.21$) tracer-flow response of silica particles to the activity of the Janus particle and the corresponding Pe_t values (color-coded background). The results shown correspond to different ratios β_i of the phoretic mobilities of the inert (silica) and active (Pt) sides; the phoretic mobility of the tracer is equal to that of the inert part of the Janus particle. The red circles indicate the in-plane ($h_{tr} = 0.21$) exclusion zone (of radii ~ $0.8R$) for the center of the tracer due to the hard-core interaction of the tracer (radius $0.2R$) with the Janus particle of radius R. The half-black–half-gray disk shows the cut by the h_{tr} plane through the Janus particle.

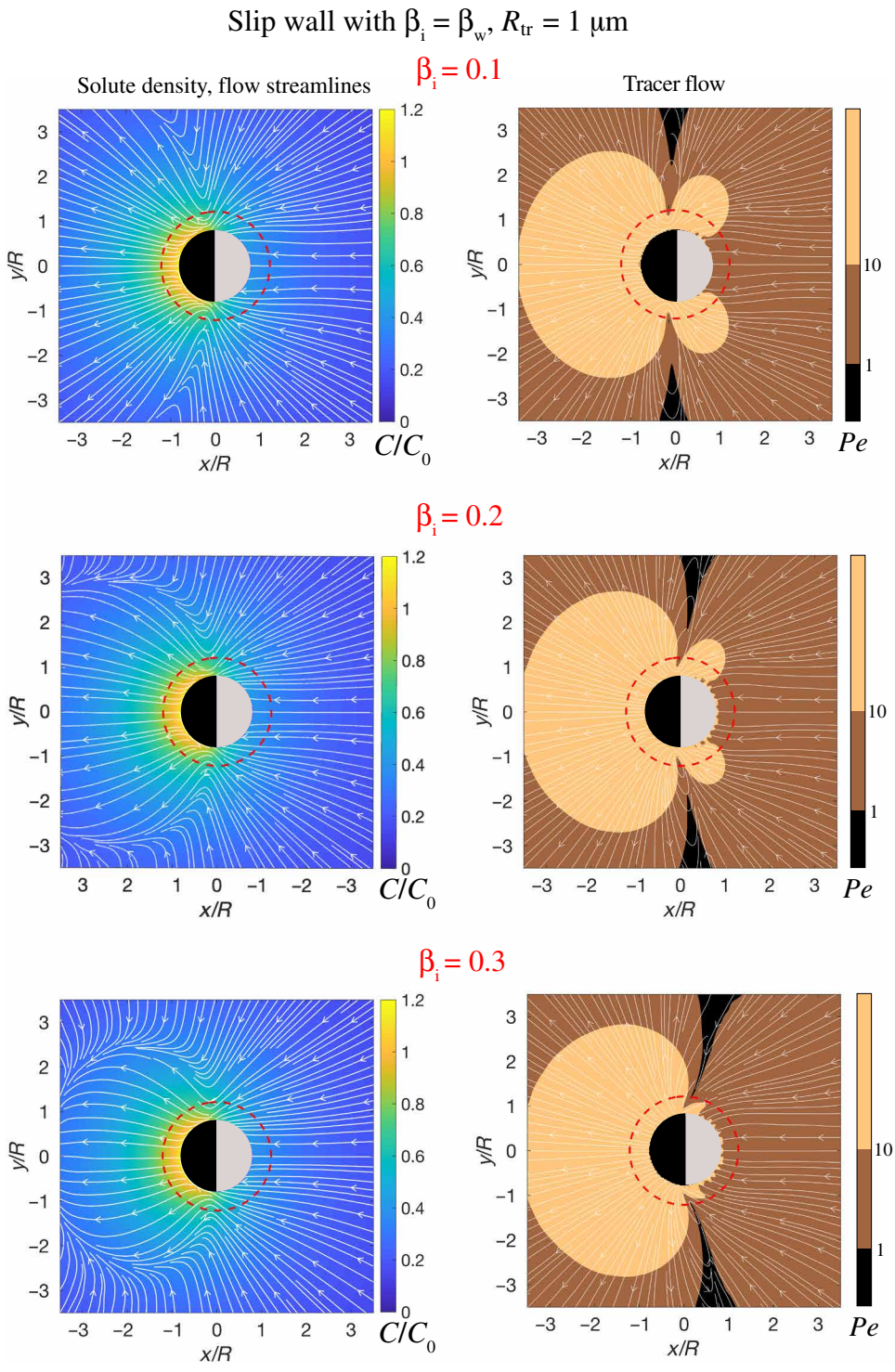

Fig. 8. Chemical field, hydrodynamic flow, and the emergent tracer dynamics around an immobile active Janus particle in a cap-parallel configuration near a wall with phoretic mobility coefficient $b_w = b_i$ for tracer size R_{tr} = 1.0 μm. Left column: $x - y$ in-plane ($z_t/R = h_{tr} = 0.41$) and dimensionless (in units of C_0) solute density (color-coded) and hydrodynamic flow streamlines corresponding to the immobile silica/Pt Janus particle located at $h/R = 1.1$. **Right column:** x-y in-plane ($z_t/R = h_{tr} = 0.41$) tracer-flow response of silica particles to the activity of the Janus particle and the corresponding Pe_t values (color-coded background). The results shown correspond to different ratios β_i of the phoretic mobilities of the inert (silica) and active (Pt) sides; the phoretic mobility of the tracer is equal to that of the inert part of the Janus particle. The red circles indicate the in-plane ($h_{tr} = 0.41$) exclusion zone (of radii ~ $1.2R$) for the center of the tracer due to the hard-core interaction of the tracer (radius $0.4R$) with the Janus particle of radius R. The half-black–half-gray disk shows the cut by the h_{tr} plane through the Janus particle.

tracer toward the equator. Therefore, in the case of an unbounded immobile Janus particle, we expect continuous pumping of tracer particles from the solution to the inert side, from the inert side to the catalytic side, and then from the catalytic side to the solution behind the Janus particle. We thus conclude that accounting for the presence of the wall is essential to recover the qualitative behavior observed in the experiments for the case of cap-parallel configuration.

DISCUSSION

To summarize, we have used the response of spherical, inert silica particles (tracers) to gain insight into the nature of the hydrodynamic and chemical fields associated with the chemical activity to a spherical active Pt/silica Janus particle under confinement. The study used active particles that are either immobilized at a glass wall in a configuration with the symmetry axis being perpendicular or parallel to the wall, or motile active particles in a state of sliding along the wall. The experiments revealed that the response of the tracer particles is strongly dependent on the configuration (i.e., orientation of the symmetry axis relative to the wall) and on the state (immobilized or motile) of the active Janus particle.

For the case of an immobilized Janus particle in a cap-up configuration, we observed the tracers experiencing an in-plane radially symmetric, effective attraction with a range of a few radii of the particle and of sufficiently large magnitude to induce the formation of close-packed ring structures around the active particle. Distinctively, for the case of an immobilized Janus particle in an axis-parallel configuration, the effective interaction experienced by the tracers is strongly anisotropic, and its character is attractive along certain direction (in particular near the inert silica side) and repulsive along the other (in particular leading to the formation of a well-defined exclusion zone at the active Pt side).

The tracer motion in the case of immobilized Janus particles is amenable to theoretical analysis at the single-particle level (dilute limit) upon choosing a model for the chemical activity and of the mechanism of self-motility, here assumed to be that of self-phoresis. Owing to the specific choice of particles and walls—in that the tracers and the core of the Janus particle are made of the same material (silica), and the wall is made of glass (also silica)—the number of the material parameters entering in the theoretical models is sufficiently decreased as to allow for a rather systematic investigation. We have shown that the experimental observations can be qualitatively captured and rationalized by a simple model of a chemically active particle and activity-induced phoretic (or osmotic) flows. This agreement could be obtained only upon accounting for the distortion by the wall of the hydrodynamic and chemical fields around the particle, as well as for an osmotic flow at the wall in response to the chemical activity of the particle. The necessity of accounting for the latter is in agreement with the similar conclusions reported in (*25*) for the conceptually similar setup, but with thermoresponsive, rather than chemically active, particles immobilized in an axis-parallel configuration. In contrast to the claims made in (*26*), we find it to be unlikely that the response of tracers can be attributed solely to the hydrodynamic flow associated with the self-motility; rather, it includes substantial contributions from phoresis in the chemical field and advection by the wall-driven osmotic flow. [The study in (*26*) additionally assumes that the tracers used there would not respond by phoresis. This is argued on the basis of additional experiments in which no motion was observed for tracers near a completely catalytic, spherical active particle immobilized at the wall. However, in such configuration, the confinement of the chemical field by the wall implies chemical gradients along the surface of the active particle and, consequently, hydrodynamic flow in the solution; accordingly, the tracers should actually exhibit motion. The reasons for this inconsistency remain unclear.] Moreover, a series of experiments using the same Janus particles, tracer particles, and solution composition, but substrates with different material composition, revealed a clear dependence of tracer dynamics on the substrate material. This dependence, which cannot occur for a no-slip wall, could be captured within our model as being due to different material-dependent osmotic flows on the substrate. In addition, the cross-checks provided by the availability of experimental results from independent, considerably different configurations (axis-perpendicular and axis-parallel, respectively) allow strong bounds to be placed on the values of the ratios of phoretic mobilities, parameters that otherwise are difficult to estimate.

We emphasize that the theoretical framework used is rather general; it assumes a simple heuristic model of a "constant flux" chemical activity for a diffusing field $c(\mathbf{x})$ and the emergence of motion via an active slip at boundaries proportional to the gradients in $c(\mathbf{x})$. These models depend only on the phoretic mobility parameters (the set of b_k in this work), which are system specific but, unfortunately, not a priori known. We expect that a similar framework may describe diverse systems, e.g., titania tracers near a Pt/silica Janus particle at a glass wall or silica tracers near an enzyme/silica Janus particle. However, there is no reason why the same set of parameters b_k would describe each distinct physical system. Determining values of these parameters is therefore an outcome of modeling. Overall, we expect active response of confining surfaces to be a generic phenomenon for chemically active colloids.

Despite the encouraging robust qualitative agreement between the model and the experiment, a word of caution is yet in order. Even in the dilute limit, within which our analysis is set up, once a ring structure forms around the immobilized Janus particle, it is not possible to rigorously argue that this would not distort the chemical and hydrodynamic fields of the Janus particle. On the other hand, it may be the case that such distortion does not play a role because the system (and the relevant fields) remains essentially three dimensional, while the tracers are within the two-dimensional monolayer. However, it has to be acknowledged that such an assumption cannot be justified a priori but only a posteriori judged in terms of the results being reasonable or not. From this perspective, further cross-validation via (computationally very expensive) numerical methods accounting explicitly for the finite size of the tracers will be very useful.

Last, we note that, in addition to capturing the experimental observations, the theoretical analysis revealed an intriguing aspect of these effective interactions involving chemically active particles, discussed in detail in note S4. This is the fact that the effective attraction, observed when the particles are near the wall (under confinement), does not carry over to the case when the particles are in unbounded solution. In the absence of confining solid boundaries, tracers would exhibit purely repulsive interactions with an active Janus particle, irrespective of whether the Janus particle is immobilized or motile.

METHODS

Experimental methods

The chemically active Janus particles used in our experiments are obtained by coating a hemisphere of silica particles (radius $R = 2.5$ μm)

with a thin layer of Pt (≈15 nm thickness). When these particles are suspended in an aqueous solution of H_2O_2, the Pt side catalyzes the degradation of H_2O_2 into water and oxygen, while, at the silica side, no chemical reactions take place. Aside from thermal fluctuations (Brownian motion), far from boundaries, the particle translates along its symmetry axis, with the Pt side at the back, i.e., it translates parallel to **d**.

To set up wall-immobilized Janus particles, the Janus particles are suspended in highly deionized water, and a droplet of the colloidal suspension is placed on a clean glass slide. Because the particles have a density considerably larger than that of water ($\rho_{SiO_2} \approx 2200$ kg/m^3), they quickly sediment onto the glass surface; the density of the Pt being a factor of ≈10 larger than that of the silica core ($\rho_{Pt} \approx 21{,}450$ kg/m^3), the configuration of the sedimented particles is somewhat biased toward that of the Pt cap facing the glass. The sample is then rapidly dried through evaporation by placing the glass slide above a hot plate (80°C), and the Janus particles adhere to the glass surface. Scanning electron microscopy imaging reveals a broad distribution for the orientation of the Janus particles stuck on the glass substrate after the drying step, including the desired axis-perpendicular and axis-parallel ones (see fig. S9).

Video analysis to extract trajectories in comoving frame

To extract from the video recording the trajectories of the tracers in the comoving reference frame, the following image analysis steps are followed. For each frame, the location of the center of the particle and the in-plane orientation of the particle, i.e., the angle between the horizontal direction of the frame and the director **d** [which is determined as the direction perpendicular to the line, clearly visible under an optical microscope in a bright-field setting (Fig. 3A), separating the silica and Pt halves], are identified. Subsequently, the pixels are reindexed such that the origin of the frame coincides with the center of the particle, which is followed by a $-\phi$ in-plane rotation of the frame. The so-modified frames are then processed to extract the trajectories of the visible tracers.

Theoretical model

We consider the following simple continuum model of chemical gradients and hydrodynamic flow created by an immobile, catalytically active Janus particle near a planar wall. The catalytic cap of the particle emits a solute molecule (i.e., oxygen) at a constant and uniform rate κ. The solute diffuses in the surrounding solution with diffusion coefficient D. The solute number density field is denoted by $c(\mathbf{x})$, where $\mathbf{x}$ is a position in the solution. The planar wall, located at $z = 0$, as well as the particle surface are impenetrable to solute. We assume that the solute Péclet number $Pe \equiv U_0 R/D \ll 1$ (where R is the radius of the particle and U_0 is a characteristic particle velocity) and that we can treat the distribution of solute as ideal gas. Hence, further assuming a fast relaxation of the distribution (quasi–steady state), $c(\mathbf{x})$ is governed by the Laplace equation $\nabla^2 c = 0$, subject to the boundary conditions $-D[\nabla c \cdot \hat{\mathbf{n}}] = \kappa$ on the catalytic cap and $-D[\nabla c \cdot \hat{\mathbf{n}}] = 0$ on both the wall and the inert face of particle. Here, the surface normal $\hat{\mathbf{n}}$ is defined to point into the liquid solution. Note that our model neglects details of the catalytic reaction, including the possible presence of charged intermediates (*34*, *39*–*43*), but we anticipate that it will capture the basic physics of flows driven by chemical gradients (*44*).

To describe these flows, we use the classical theory of neutral diffusiophoresis (*32*, *33*). The interaction of solute molecules with a bounding solid surface drives flow in a thin layer adjacent to the surface. These surface flows are modeled by an effective slip velocity $\mathbf{v}_s(\mathbf{x}_s) = -b(\mathbf{x}_s)\nabla_{\|} c$, where $\mathbf{x}_s$ is a position on a bounding solid surface and $\nabla_{\|} \equiv (\mathbf{I} - \hat{\mathbf{n}}\hat{\mathbf{n}}) \cdot \nabla$ is the surface gradient operator. The quantity $b(\mathbf{x}_s)$, the so-called surface or phoretic mobility, is a material-dependent parameter that encapsulates the details of the solute/surface interaction potential. We take $b(\mathbf{x}_s)$ to be piecewise constant, with $b(\mathbf{x}_s) = b_w$ on the solid wall, $b(\mathbf{x}_s) = b_c$ on the catalytic cap, and $b(\mathbf{x}_s) = b_i$ on the inert face of the particle because these three surface regions can be made of distinct materials.

The surface flows drive flow in the bulk solution. Assuming that the Reynolds number $Re \equiv \rho U_0 R/\mu \ll 1$, where μ is the viscosity of the solution and ρ is the fluid density, we take the fluid velocity $\mathbf{u}(\mathbf{x})$ to be governed by the incompressible Stokes equation $-\nabla P + \mu\nabla^2\mathbf{u} = 0$, $\nabla \cdot \mathbf{u} = 0$, where $P(\mathbf{x})$ is the fluid pressure. The fluid velocity, $\mathbf{u}(\mathbf{x})$, is subject to the boundary conditions $\mathbf{u} = \mathbf{v}_s(\mathbf{x}_s)$ on the wall and on the surface of the particle. The particle is assumed to be motionless because of being irreversibly adsorbed at the planar wall. Implicitly, the constraining interaction force $\mathbf{F}_c$ balances the hydrodynamic force $\mathbf{F}_h = \int \sigma \cdot \hat{\mathbf{n}}\, dS$ on the particle, such that $\mathbf{F}_c + \mathbf{F}_h = 0$ (and similarly, a constraining torque $\mathbf{T}_c$ balances the hydrodynamic one). Here, the stress tensor is Newtonian, i.e., $\sigma = -P\mathbf{I} + \mu[\nabla \mathbf{u} + (\nabla \mathbf{u})^T]$. Overall, the Laplace and Stokes equations, in conjunction with their respective boundary conditions, can be solved numerically (via the boundary element method) or, for geometric configurations with high symmetry, analytically.

At this point, we highlight that our model considers hydrodynamic flow driven by both phoretic slip on the particle surface and chemiosmotic slip on the planar wall. These chemiosmotic flows should generically occur whenever chemically active particles operate near confining solid boundaries because chemiosmotic and diffusiophoretic flows are ultimately driven by the same interfacial mechanism (*30*, *45*, *46*). While the importance of osmotic flows has been emphasized in studies of chemically active pumps (*47*–*51*), such activity-induced chemiosmotic flow—which, as follows, may be an essential ingredient for coherently capturing the phenomenology observed in experiments [see also (*25*)]—is often neglected (*26*, *52*) in the hydrodynamic modeling of chemically active particles.

Because the Stokes equation is linear, we can decompose the hydrodynamic flow into separate contributions from phoretic slip on the particle and chemiosmotic slip on the wall: $\mathbf{u} = \mathbf{u}_p + \mathbf{u}_w$. (This decomposition will allow us to distinguish and isolate the physical effects of phoretic slip and chemiosmotic slip.) The quantity $\mathbf{u}_p$ is obtained by solving the problem posed in the preceding paragraphs, but with $b_w = 0$. Similarly, $\mathbf{u}_w$ can be obtained by solving the problem posed above, with $b_w \neq 0$ but $b_c = 0$ and $b_i = 0$.

Concerning the use of the boundary element method, we note that, to determine the osmotic-driven flows, it is necessary to mesh both the surface of the Janus particle and the surface of the wall. The wall is treated as a finite-sized slab with thickness $0.75R$ and width $20R$. The wall mesh is locally refined in the vicinity of the Janus particle to ensure that negligible solute concentration leaks through the wall, i.e., the solute concentration below the lower surface of the wall is negligible. Concerning the boundary conditions for the slab-like wall, we specify (as for the infinite planar wall discussed above) that the wall is impenetrable to solute and that the surface of the wall has surface mobility b_w. In addition to checking that the solute concentration below the wall is negligible, we have validated our mesh by recovering the analytical results for the cap-perpendicular configuration.

In addition, we note that our numerical calculations approximately reproduce the expected mirror symmetry, with respect to the particle symmetry axis, of the concentration and flow fields; however, slight asymmetries in the flow field can be observed near stagnation points, which are particularly sensitive to discretization error. (The Janus particle mesh is mirror symmetric, but the wall mesh is not.) For the same reason, the border between different regions of the tracer Péclet number may appear as a somewhat rough, rather than smooth, curve.

Within the framework of our numerical model, velocities are computed in terms of a characteristic velocity $U_0 = |b_c\kappa/D|$, e.g., tracer velocities are determined as a dimensionless ratio $\mathbf{v}_t/U_0$. For the activity profile assumed here (i.e., a constant and uniform rate on the cap), the velocity of an isolated motile Janus particle in unbounded solution (i.e., far from confining surfaces) is $U_{fs}/U_0 = \frac{1}{8}(1 + \beta_i)$, where $\beta_i = b_i/b_c$ (*53*). To estimate the tracer Péclet number $Pe_t = |\mathbf{v}_t| R_{tr}/D_{tr}$, and informed by experimental observations of Janus particle speeds, we take $U_{fs} \sim 5$ μm/s in dimensional units, which allows estimation of U_0 in units of μm/s (for any particular choice of β_i.) In this manner, dimensional values of $\mathbf{v}_t$ can be obtained from the dimensionless ratio $\mathbf{v}_t/U_0$ and substituted into $Pe_t = |\mathbf{v}_t| R_{tr}/D_{tr}$.

Last, we note that, as discussed in the "Theoretical interpretation" part [see the text around eq (1)], the location of the Janus particle was slightly shifted vertically, i.e., a value $h/R > 1$ has been used. This is necessary to avoid the technical and numerical difficulties related to the accuracy of the numerical solutions near the contact point between the sphere and the wall. We have checked for the cap-perpendicular configurations, by comparing the results corresponding to using $h/R = 1.1$ and $h/R = 1.05$, respectively, that the exact value of this shift does not qualitatively influence the results.

SUPPLEMENTARY MATERIALS

Supplementary material for this article is available at http://advances.sciencemag.org/cgi/content/full/7/18/eabd0719/DC1

REFERENCES AND NOTES

1. W. F. Paxton, S. Sundararajan, T. E. Mallouk, A. Sen, Chemical locomotion. *Angew. Chem. Int. Ed.* **45**, 5420–5429 (2006).
2. S. J. Ebbens, J. R. Howse, In pursuit of propulsion at the nanoscale. *Soft Matter* **6**, 726–738 (2010).
3. S. Ramaswamy, The mechanics and statistics of active matter. *Annu. Rev. Condens. Matter Phys.* **1**, 323–345 (2010).
4. A. Bricard, J.-B. Caussin, N. Desreumaux, O. Dauchot, D. Bartolo, Emergence of macroscopic directed motion in populations of motile colloids. *Nature* **503**, 95–98 (2013).
5. G. Kokot, A. Snezhko, Manipulation of emergent vortices in swarms of magnetic rollers. *Nat. Commun.* **9**, 2344 (2018).
6. J. Palacci, S. Sacanna, A. P. Steinberg, D. J. Pine, P. M. Chaikin, Living crystals of light-activated colloidal surfers. *Science* **339**, 936–940 (2013).
7. F. Ginot, I. Theurkauff, F. Detcheverry, C. Ybert, C. Cottin-Bizonne, Aggregation-fragmentation and individual dynamics of active clusters. *Nat. Commun.* **9**, 696 (2018).
8. I. Theurkauff, C. Cottin-Bizonne, J. Palacci, C. Ybert, L. Bocquet, Dynamic clustering in active colloidal suspensions with chemical signaling. *Phys. Rev. Lett.* **108**, 268303 (2012).
9. I. Buttinoni, J. Bialke, F. Kummel, H. Lowen, C. Bechinger, T. Speck, Dynamical clustering and phase separation in suspensions of self-propelled colloidal particles. *Phys. Rev. Lett.* **110**, 238301 (2013).
10. A. Aubret, M. Youssef, S. Sacanna, J. Palacci, Targeted assembly and synchronization of self-spinning microgears. *Nat. Phys.* **14**, 1114–1118 (2018).
11. J. Yan, M. Han, J. Zhang, C. Xu, E. Luijten, S. Granick, Reconfiguring active particles by electrostatic imbalance. *Nat. Mater.* **15**, 1095–1099 (2016).
12. F. Kummel, P. Shabestari, C. Lozano, G. Volpe, C. Bechinger, Formation, compression and surface melting of colloidal clusters by active particles. *Soft Matter* **11**, 6187–6191 (2015).
13. D. P. Singh, U. Choudhury, P. Fischer, A. G. Mark, Non-equilibrium assembly of light-activated colloidal mixtures. *Adv. Mater.* **29**, 1701328 (2017).
14. H. Massana-Cid, J. Codina, I. Pagonabarraga, P. Tierno, Active apolar doping determines routes to colloidal clusters and gels. *Proc. Natl. Acad. Sci. U.S.A.* **115**, 10618–10623 (2018).
15. H. H. Wensink, H. Lowen, Aggregation of self-propelled colloidal rods near confining walls. *Phys. Rev. E* **78**, 031409 (2008).
16. W. E. Uspal, M. N. Popescu, S. Dietrich, M. Tasinkevych, Self-propulsion of a catalytically active particle near a planar wall: From reection to sliding and hovering. *Soft Matter* **11**, 434–438 (2015).
17. D. Takagi, J. Palacci, A. Braunschweig, M. Shelley, J. Zhang, Hydrodynamic capture of microswimmers into sphere-bound orbits. *Soft Matter* **10**, 1784–1789 (2016).
18. M. N. Popescu, W. E. Uspal, A. Domnguez, S. Dietrich, Effective interactions between chemically active colloids and interfaces. *Acc. Chem. Res.* **51**, 2991–2997 (2018).
19. S. Das, A. Garg, A. I. Campbell, J. Howse, A. Sen, D. Velegol, R. Golestanian, S. J. Ebbens, Boundaries can steer active Janus spheres. *Nat. Commun.* **6**, 8999 (2015).
20. J. Simmchen, J. Katuri, W. E. Uspal, M. N. Popescu, M. Tasinkevych, S. Sanchez, Topographical pathways guide chemical microswimmers. *Nat. Commun.* **7**, 10598 (2016).
21. C. Maggi, J. Simmchen, F. Saglimbeni, J. Katuri, M. Dipalo, F. De Angelis, S. Sanchez, R. Di Leonardo, Self-assembly of micromachining systems powered by Janus micromotors. *Small* **12**, 446–451 (2016).
22. J. Katuri, D. Caballero, R. Voituriez, J. Samitier, S. Sanchez, Directed flow of micromotors through alignment interactions with micropatterned ratchets. *ACS Nano* **12**, 7282–7291 (2018).
23. J. Palacci, S. Sacanna, A. Abramian, J. Barral, K. Hanson, A. Y. Grosberg, D. J. Pine, P. M. Chaikin, Artificial rheotaxis. *Sci. Adv.* **1**, e1400214 (2015).
24. J. Katuri, W. E. Uspal, J. Simmchen, A. Miguel-Lopez, S. Sanchez, Cross-stream migration of active particles. *Sci. Adv.* **4**, eaao1755 (2018).
25. A. P. Bregulla, F. Cichos, Flow fields around pinned self-thermophoretic microswimmers under confinement. *J. Chem. Phys.* **151**, 044706 (2019).
26. A. I. Campbell, S. J. Ebbens, P. Illien, R. Golestanian, Experimental observation of flow fields around active Janus spheres. *Nat. Commun.* **10**, 3952 (2018).
27. A. Varma, S. Michelin, Modeling chemo-hydrodynamic interactions of phoretic particles: A unified framework. *Phys. Rev. Fluids* **4**, 124204 (2019).
28. A. I. Campbell, S. J. Ebbens, Gravitaxis in spherical Janus swimming devices. *Langmuir* **29**, 14066–14073 (2013).
29. S. Das, Z. Jalilvand, M. N. Popescu, W. E. Uspal, S. Dietrich, I. Kretzschmar, Floor- or ceiling-sliding for chemically active, gyrotactic, sedimenting Janus particles. *Langmuir* **36**, 7133–7147 (2020).
30. W. E. Uspal, M. N. Popescu, S. Dietrich, M. Tasinkevych, Guiding catalytically active particles with chemically patterned surfaces. *Phys. Rev. Lett.* **117**, 048002 (2016).
31. W. E. Uspal, M. N. Popescu, M. Tasinkevych, S. Dietrich, Shape-dependent guidance of active Janus particles by chemically patterned surfaces. *New J. Phys.* **20**, 015013 (2018).
32. J. L. Anderson, Colloid transport by interfacial forces. *Annu. Rev. Fluid Mech.* **21**, 61–99 (1989).
33. R. Golestanian, T. B. Liverpool, A. Ajdari, Designing phoretic micro- and nano-swimmers. *New J. Phys.* **9**, 126 (2007).
34. A. T. Brown, W. C. K. Poon, C. Holm, J. de Graaf, Ionic screening and dissociation are crucial for understanding chemical self-propulsion in polar solvents. *Soft Matter* **13**, 1200–1222 (2017).
35. H. Brenner, The slow motion of a sphere through a viscous uid towards a plane surface. *Chem. Eng. Sci.* **16**, 242–251 (1961).
36. G. B. Jeffery, On a form of the solution of Laplace's equation suitable for problems relating to two spheres. *Proc. R. Soc. A* **87**, 109–120 (1912).
37. D. Papavassiliou, G. P. Alexander, Exact solutions for hydrodynamic interactions of two squirming spheres. *J. Fluid Mech.* **813**, 618–646 (2017).
38. J. Happel, H. Brenner, *Low Reynolds Number Hydrodynamics* (Prentice-Hall, 1965).
39. A. Brown, W. C. K. Poon, Ionic effects in self-propelled Pt-coated Janus swimmers. *Soft Matter* **10**, 4016–4027 (2014).
40. S. Ebbens, D. A. Gregory, G. Dunderdale, J. R. Howse, Y. Ibrahim, T. B. Liverpool, R. Golestanian, Electrokinetic effects in catalytic platinum-insulator Janus swimmers. *EPL* **106**, 58003 (2014).
41. A. T. Brown, I. D. Vladescu, A. Dawson, T. Vissers, J. Schwarz-Linek, J. S. Lintuvuori, W. C. K. Poon, Swimming in a crystal. *Soft Matter* **12**, 131–140 (2016).
42. A. Brooks, M. Tasinkevych, S. Sabrina, D. Velegol, A. Sen, K. J. M. Bishop, Shape-directed rotation of homogeneous micromotors via catalytic self-electrophoresis. *Nat. Commun.* **10**, 459 (2019).
43. M. De Corato, X. Arque, T. Patino, M. Arroyo, S. Sanchez, I. Pagonabarraga, Self-propulsion of active colloids via ion release: Theory and experiments. *Phys. Rev. Lett.* **124**, 108001 (2020).
44. J. R. Howse, R. A. L. Jones, A. J. Ryan, T. Gough, R. Vafabakhsh, R. Golestanian, Self-motile colloidal particles: From directed propulsion to random walk. *Phys. Rev. Lett.* **99**, 048102 (2007).

45. T.-Y. Chiang, D. Velegol, Localized electroosmosis (leo) induced by spherical colloidal motors. *Langmuir* **30**, 2600–2607 (2014).
46. J. Palacci, S. Sacanna, S.-H. Kim, G.-R. Yi, D. Pine, P. Chaikin, Light-activated self-propelled colloids. *Phil. Trans. R. Soc. A* **372**, 20130372 (2014).
47. A. A. Farniya, M. J. Esplandiu, D. Reguera, A. Bachtold, Imaging the proton concentration and mapping the spatial distribution of the electric field of catalytic micropumps. *Phys. Rev. Lett.* **111**, 168301 (2013).
48. A. P. Bregulla, A. Wurger, K. Gunther, M. Mertig, F. Cichos, Thermo-osmotic flow in thin films. *Phys. Rev. Lett.* **116**, 188303 (2016).
49. R. Niu, T. Palberg, T. Speck, Self-assembly of colloidal molecules due to self-generated flow. *Phys. Rev. Lett.* **119**, 028001 (2017).
50. R. Niu, P. Kreissl, A. T. Brown, G. Rempfer, D. Botin, C. Holm, T. Palberg, J. de Graaf, Microuidic pumping by micromolar salt concentrations. *Soft Matter* **13**, 1505–1518 (2017).
51. R.-E. Munteanu, M. N. Popescu, S. Gaspar, Glucose Oxidase micropumps: Multi-faceted effects of chemical activity on tracer particles near the solid-liquid interface. *Condens. Matter* **4**, 73 (2019).
52. E. Kanso, S. Michelin, Phoretic and hydrodynamic interactions of weakly confined autophoretic particles. *J. Chem. Phys.* **150**, 044902 (2019).
53. M. N. Popescu, W. E. Uspal, Z. Eskandari, M. Tasinkevych, S. Dietrich, Effective squirmer models for self-phoretic chemically active spherical colloids. *Eur. Phys. J. E* **41**, 145 (2018).
54. M. N. Popescu, W. E. Uspal, C. Bechinger, P. Fischer, Chemotaxis of active Janus nanoparticles. *Nano Lett.* **18**, 5345–5349 (2018).

Acknowledgments: We would like to thank an anonymous reviewer for the suggestion of complementary experiments involving different materials. We would also like to thank À. Blanco for assistance in fabrication of samples necessary for these experiments. **Funding:** The research has received funding from CERCA Programme/Generalitat de Catalunya, Secretaria d'Universitats i Recerca del Departament d'Empresa i Coneixement de la Generalitat de Catalunya through the project 2017 SGR 1148; Ministerio de Ciencia, Innovación y Universidades (MCIU)/Agencia Estatal de Investigación (AEI)/Fondo Europeo de Desarrollo Regional (FEDER, UE) through the project RTI2018-098164-B-I00; and the European Research Council (ERC) under the European Union's Horizon 2020 research and innovation program (grant agreement no. 866348: iNanoSwarms). W.E.U. acknowledges donors of the American Chemical Society Petroleum Research Fund for partial support of this research through grant no. 60809-DNI9. S.S. thanks the Pengcheng Scholar Professorship at Harbin Institute of Technology Shenzhen, China. J.K. is currently affiliated with Argone National Laboratory, 9700 S. Cass Avenue, Lemont, IL 60439, USA. **Author contributions:** All authors conceived the idea of the project and contributed to the writing of the paper. J.K. performed the experiments supervised by S.S. W.E.U. and M.N.P. performed the theoretical modeling. J.K., W.E.U., and M.N.P. analyzed and interpreted the data. **Competing interests:** The authors declare that they have no competing interests. **Data and materials availability:** All data needed to evaluate the conclusions in the paper are present in the paper and/or the Supplementary Materials.

Submitted 31 May 2020
Accepted 12 March 2021
Published 30 April 2021
10.1126/sciadv.abd0719

Citation: J. Katuri, W. E. Uspal, M. N. Popescu, S. Sánchez, Inferring non-equilibrium interactions from tracer response near confined active Janus particles. *Sci. Adv.* **7**, eabd0719 (2021).

ScienceAdvances

Inferring non-equilibrium interactions from tracer response near confined active Janus particles

Jaideep KaturiWilliam E. UspalMihail N. PopescuSamuel Sánchez

Sci. Adv., 7 (18), eabd0719. • DOI: 10.1126/sciadv.abd0719